Journal of Alloys and Compounds 509 (2011) L90–L94

Contents lists available at ScienceDirect

Journal of Alloys and Compounds

journal homepage: www.elsevier.com/locate/jallcom

Letter

In situ nanostructured ceramic matrix composite coating prepared by reactive plasma spraying micro-sized Al–Fe_2O_3 composite powders

Yong Yang*, Dianran Yan, Yanchun Dong, Lei Wang, Xueguang Chen, Jianxin Zhang, Jining He, Xiangzhi Li

School of Materials Science and Engineering, Hebei University of Technology, Tianjin, PR China

ARTICLE INFO

Article history:
Received 4 October 2010
Received in revised form
22 November 2010
Accepted 22 November 2010
Available online 30 November 2010

Keywords:
Coating materials
Composite materials
Nanostructured materials
Solid state reaction
Mechanical properties
Reactive plasma spraying (RPS)

ABSTRACT

In situ nanostructured ceramic matrix composite coating was prepared by reactive plasma spraying micro-sized Al–Fe_2O_3 composite powders. The microstructure of the composite coating was characterized by X-ray diffraction, scanning electron microscopy and transmission electron microscopy, respectively. The results indicated that the composite coating exhibited dense and crack-free microstructure with a number of spherical α-Fe and γ-Al_2O_3 nano-grains embedded within equiaxed and columnar $FeAl_2O_4$ nano-grains matrix. The composite coating showed markedly higher toughness and wear resistance than the conventional Al_2O_3 coating.

1. Introduction

Ceramic coating is a very promising approach to tailor the surface properties of metal component due to their high hardness, excellent wear, corrosion, chemical and thermal resistance [1]. However, one of the inherent drawbacks of ceramic coating is its brittleness, which limits its more widely application. Therefore, many toughening methods have been put forward, in which the inclusion of second phases into ceramic coating was widely investigated [2]. Ceramic matrix composite (CMC) coatings, especially metal toughened CMC coatings, exhibited enhanced toughness and wear resistance compared with monolithic ceramic coatings [3,4]. On the other hand, increasing efforts have been recently directed towards the synthesis of nanostructured materials because novel and exciting physical, chemical and mechanical properties can be expected [5,6]. Nanostructured CMC coatings have been considerably investigated and reported to possess superior toughness, adhesion, spallation, wear, corrosion and thermal resistance compared to their conventional coarse-grained counterparts [7–9].

A number of techniques have been attempted to produce nanostructured coatings, such as physical vapor deposition, chemical vapor deposition, ion implantation, magnetron sputtering, electrodeposition, laser cladding, thermal spraying and cold spraying [6,10–14]. Among the possible processes, reactive plasma spraying (RPS), which combines plasma spraying with self-propagating high-temperature synthesis to produce *in situ* composite coatings, has received much attention in recent years [15,16]. The principle of RPS is based on the reaction between feedstock materials or between feedstock materials and surrounding reactive gases present in the plasma. RPS has numerous advantages [15–21]: (i) simplicity of the process; (ii) high deposition rate and hence the possibility of preparing thick (up to several hundreds of microns or more) and scaleable coatings; (iii) improved cohesive strength between second phases and matrix due to *in situ* formation of second phases; (iv) the opportunity to form metastable or intermediate phases by combining steep thermal gradients, high reaction rates, and relatively rapid cooling rates; (v) the higher purity of products as volatile impurities are expelled due to high temperatures; and finally (vi) reduced cost, which is attributed to the possibility of substitution of expensive raw materials with cheaper ones for synthesizing the same products and relatively low energy requirement due to the significant amounts of heat released by exothermic reactions. RPS, therefore, offers much scope in the commercial production of multi-component composite thick coatings with improved properties. However, to the best knowledge of authors, there is little information about the synthesis of nanostrucutured CMC coating using RPS.

* Corresponding author at: No. 29 Guangrong Road, Hongqiao District, Tianjin 300132, PR China. Tel.: +86 22 60204581; fax: +86 22 26564581.
E-mail addresses: yangyonghebut@163.com, hityangyong@163.com (Y. Yang).

0925-8388/$ – see front matter © 2010 Elsevier B.V. All rights reserved.
doi:10.1016/j.jallcom.2010.11.167

Table 1
The main plasma spraying parameters.

	Voltage (V)	Current (A)	primary gas (Ar) flow rate (L min^{-1})	secondary gas (H_2) flow rate (L min^{-1})	Spray distance (mm)
Al_2O_3 coating	75	500	80	20	80–100
Composite coating	60	500	80	20	80–100

In this letter, we report, for the first time, a simple but efficient approach that uses reactive plasma spraying *micro-sized* Al–Fe_2O_3 composite powders to prepare *in situ* high-performance *nanostructured* CMC coating toughened by metallic phase. The microstructure and mechanical properties of the as-sprayed nanostructured CMC coating were carefully characterized.

2. Materials and methods

RPS in the present investigation is based on the thermite reaction of Al–Fe_2O_3 system. As-received powders are Fe_2O_3 (analytical grade, Tianjin Third Chemical Reagent Co., Ltd., China) with average grain size about 0.6–0.8 μm and Al (99.9% grade, Anshan Iron and Steel Fine Aluminum Powder Co., Ltd., China) with average grain size about 5 μm. The powders were reconstituted uniformly to produce a powder mixture with molar ratio composition of 1:2 of Fe_2O_3 and Al by wet mixing using absolute alcohol as the mixing media and polyvinyl alcohol as binder. The powder mixture was then dried at 150 °C and sieved through the sieve of 200–300 mesh. The carbon steel (0.14–0.22 wt.%C) coupons were used as substrates. A bond coating of Ni-10 wt.%Al self-melting alloy with thickness about 100 μm was deposited onto the substrates. The as-prepared Al–Fe_2O_3 composite powders and conventional micro-sized monolithic Al_2O_3 powders (for comparison) were then plasma sprayed onto the bond coatings for about 400 μm in thickness, respectively. The plasma spraying parameters were as follows: (a) primary gas (Ar) flow rate was 80 L min^{-1}, (b) secondary gas (H_2) flow rate was 20 L min^{-1}, (c) current was 500 A, (d) voltage was 60 V and (e) spray distance was 80–100 mm Table 1. Cross-sections of the as-prepared composite coating were ground and polished. Specimens for transmission electron microscopy (TEM) were prepared with grinding and ion milling to electron transparency by using a Gatan 656 dimple grinder and a Gatan 691 Ion-Miller. The phase constitution of the composite powders and as-prepared coatings were characterized by X-ray diffraction (XRD, Philips X'-Pert MPD) with Cu Kα radiation. A scanning electron microscope (SEM, Philips XL30/TMP) equipped with X-ray energy dispersive spectroscope (EDS) was employed to characterize the morphologies of the composite powders and the cross-section of the coating. The microstructure of the coating was characterized by transmission electron microscope (TEM, Philips Tec-nai F20). The microhardness was determined on the polished cross-section of the coatings by a HX-1000 Microhardness Tester under an indent load of 100 g with a dwell time of 15 s (ten indents for each sample). Relative toughness of the coatings were expressed by crack extension force (G_c) calculated from Eq. (1) [22]:

$$G_c = 6.115 \times 10^{-4} \left(a^2 \cdot \frac{P}{c^3} \right) \quad (1)$$

where, G_c: the crack extension force (J m^{-2}); a: the impression half-diagonal (m); P: the indentation load (N); c: the half of the total length (tip-to-tip) of the major crack. Unlubricated sliding wear test was performed on an M-200 tribometer (Xuanhua Material Test Machine Co., Ltd., Xuanhua, China) using block-on-ring configuration in air at room temperature. Commercial heat-treated GCr15 steel (0.95–1.05 wt.%C, 1.30–1.65 wt.%Cr) rings (HRC 62) were used to rotate in contact with each block sample. The normal load on each block was 100 N, 200 N, 300 N, 400 N and 500 N, respectively. The sliding velocity was about 0.4 m s^{-1}, and the sliding time was 30 min. The wear volume was determined using the wear track data measured by the profile meter. At least three specimens were tested for each load to obtain the average value.

3. Results and discussion

Fig. 1 shows the SEM micrograph of the composite powders. After reconstitution processing, quasi-spherical composite powders had been obtained. The average particle size of the composite powders is about 50 μm in diameter. Each feedstock particle consists of many micro-sized Al and Fe_2O_3 granules and the composite feedstock particles are compact. Such structure of the composite powders provides homogeneous distribution of Al and Fe_2O_3. Therefore, thermite reaction between Al and Fe_2O_3 may be enhanced to prepare *in situ* composite with homogeneous composition distribution [23].

The Al–Fe_2O_3 composite powders were then plasma sprayed onto the substrate. Fig. 2 shows the XRD pattern of the as-prepared

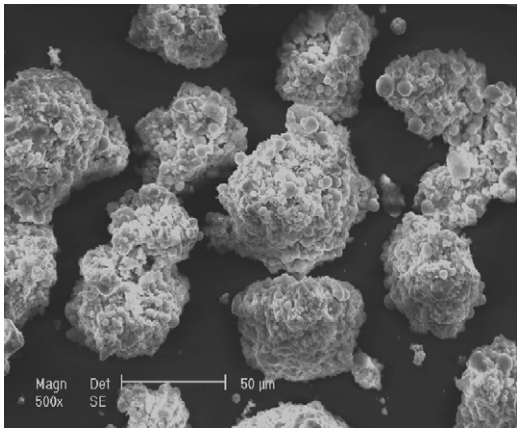

Fig. 1. SEM micrograph of the composite powders.

coating, indicating that the as-prepared coating is composed of $FeAl_2O_4$, γ-Al_2O_3 and α-Fe as a result of the thermite reaction between Al and Fe_2O_3 during plasma spraying. The molar ratio of Al/Fe_2O_3 is 2:1 in the present investigation, which will lead to reaction products Al_2O_3 and Fe under equilibrium condition according to Eq. (2) [24],

$$2Al + Fe_2O_3 = Al_2O_3 + 2Fe \quad (2)$$

However, it had been pointed out that the chemical composition and phases of the reaction products of Al–Fe_2O_3 thermite system were mainly dependent on the reactants composition, reaction extent and cooling conditions [25]. It is well known that the non-equilibrium plasma spraying process is characterized by high temperatures (~10,000 K), high velocity (about 200 m s^{-1}) and extremely high cooling rate (about 10^6–10^8 K s^{-1}) [6,14,22]. Therefore, the reaction products ($FeAl_2O_4$, Al_2O_3 and Fe), which were also reported in other non-equilibrium processing of Al–Fe_2O_3 thermite system [25–28], were different from that of the equilibrium reaction condition (Al_2O_3 and Fe).

Cross-sectional back-scattered SEM micrograph and corresponding EDS results of the CMC coating are shown in Fig. 3 and Table 2. The cross-sectional view of the CMC coating presents dense and crack-free microstructure with little porosity. Moreover, the back-scattered SEM micrograph of the CMC coating (Fig. 3)

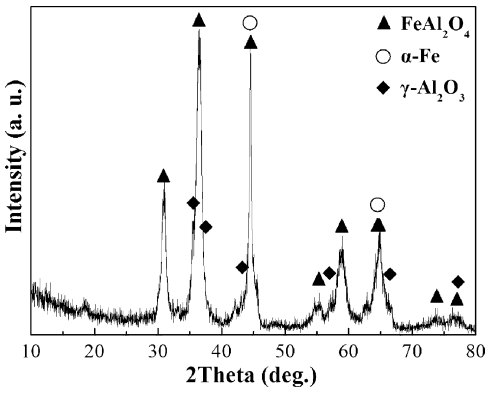

Fig. 2. XRD pattern of the CMC coating.

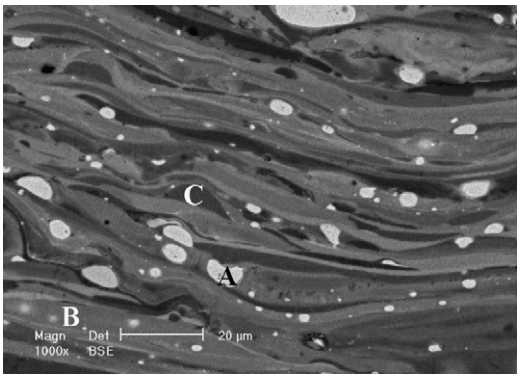

Fig. 3. Cross-sectional back-scattered SEM micrograph of the CMC coating.

indicates that the CMC coating contains three distinctive regions, namely white region (A), light gray region (B) and dark gray region (C). Table 2 shows the EDS results of corresponding regions in Fig. 3. Combined the EDS results with the XRD results (Fig. 2), it may be inferred that the white region (A) is highly rich in α-Fe, the light gray region (B) rich in $FeAl_2O_4$, and the dark gray region (C) rich in Al_2O_3. Therefore, the CMC coating could be considered to have a microstructure with thin lamellar splats rich in $FeAl_2O_4$ (light gray region) as matrix, and dispersed granules rich in α-Fe (white region) and thin lamellar splats rich in γ-Al_2O_3 (dark gray region) as second phases. It is well known that $FeAl_2O_4$ and Al_2O_3 ceramic phases are hard but brittle, while Fe metallic phase is tough and ductile. Inclusion of metallic phase Fe in $FeAl_2O_4$ ceramic matrix may, therefore, improve the toughness of the ceramic coating effectively [25–28].

Table 2
EDS results of the CMC coating corresponding to Fig. 3.

	Fe (at%)	Al (at%)	O (at%)
White region (A)	87.79	4.04	8.17
Light gray region (B)	35.60	22.32	42.08
Dark gray region (C)	18.22	32.71	49.07

TEM micrographs and the corresponding selected area diffraction (SAD) patterns of the CMC coating are shown in Fig. 4. The CMC coating consists of a great amount of nano-sized grains with different morphology, which are on the order of tens of nanometers to hundreds of nanometers. There are equiaxed grains with size about 50–200 nm in the CMC coating (Fig. 4a). The EDS result (not shown) exhibits that the equiaxed grains contain Fe, Al and O, and the SAD pattern (inserted image in Fig. 4a) of these equiaxed grains was indexed to $FeAl_2O_4$. Moreover, there are also columnar grains with diameter about 50–100 nm in the CMC coating (Fig. 4b).

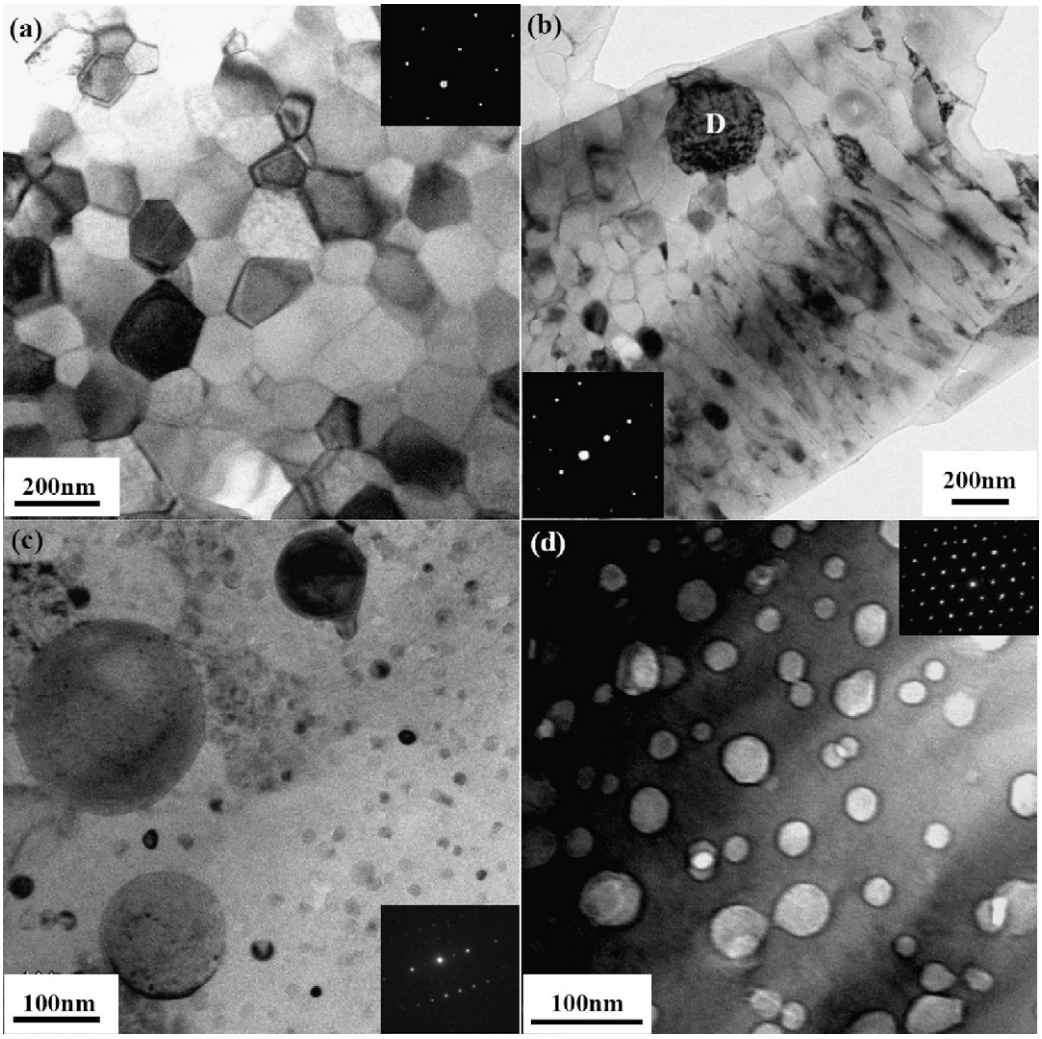

Fig. 4. TEM micrographs and the corresponding SAD patterns of the CMC coating: (a) equiaxed $FeAl_2O_4$ nano-grains, (b) equiaxed and columnar $FeAl_2O_4$ nano-grains and spherical α-Fe nano-grain, (c) spherical α-Fe nano-grains, (d) spherical γ-Al_2O_3 nano-grains.

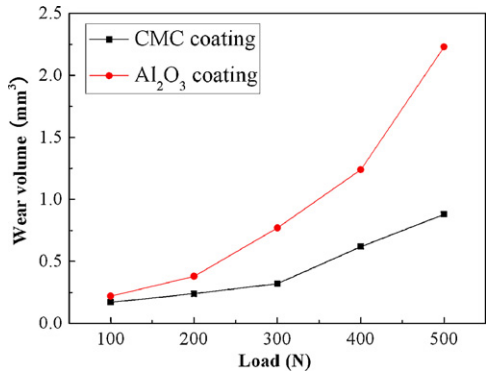

Fig. 5. Wear volume of the Al_2O_3 coating and the CMC coating at different loads.

The EDS result and the SAD pattern of these columnar grains reveal that they are $FeAl_2O_4$. It can be inferred from the above results that the microstructure in Figs. 4a and b correspond to the light gray region (B) in Fig. 3. It can be noted that there is spherical grain about 200 nm distributed within the $FeAl_2O_4$ matrix (D in Fig. 4b). The EDS result and the SAD pattern of the spherical grain suggest that it is α-Fe. There are a lot of spherical grains with size about 10–200 nm embedded within the matrix (Fig. 4c). The EDS result and the SAD pattern reveal that these spherical grains are α-Fe. It can be inferred that the microstructure in Fig. 4c corresponds to the white region (A) in Fig. 3. There are also a number of spherical grains with size about 10–60 nm embedded within the matrix (Fig. 4d), and the SAD pattern reveals that these spherical grains are γ-Al_2O_3. It can be inferred that the microstructure in Fig. 4d corresponds to the dark gray region (C) in Fig. 3. The TEM characterization results reveal that the CMC coating presents a microstructure with a number of spherical α-Fe and γ-Al_2O_3 nano-sized grains embedded within the equiaxed and columnar $FeAl_2O_4$ nano-grains matrix, which are consistent with the SEM analysis results.

In order to evaluate the properties of the CMC coating, microhardness, toughness, and wear tests were carried out. The microhardness of the CMC coating is 900 ± 30 HV, which is lower than that of conventional microstructured monolithic Al_2O_3 coating developed using plasma spraying (1070 ± 40 HV) due to presence of softer $FeAl_2O_4$ and Fe phases in the coating. However, the crack extension force (G_c) of the CMC coating and the Al_2O_3 coating are 11.3 J m^{-2} and 5.4 J m^{-2}, respectively, which indicates that the CMC coating possesses higher toughness (more than double) compared with the Al_2O_3 coating.

Fig. 5 shows the wear volume of the Al_2O_3 coating and the CMC coating against GCr15 steel at different loads. The wear volume of the two coatings increases with increasing load, respectively. The wear volume of the CMC coating is lower than that of the Al_2O_3 coating under the same load, especially under the higher load. The wear volume of the CMC coating is only one-third of that of the Al_2O_3 coating under normal load of 500 N, which means that the wear resistance of the CMC coating is enhanced by a factor of two compared with the Al_2O_3 coating. Four reasons are considered responsible for the higher wear resistance of the CMC coating in comparison with that of the Al_2O_3 coating: (a) Despite the fact that the Al_2O_3 coating has higher hardness, however, hardness is not the paramount property affecting the wear resistance of the coatings, but fracture toughness is, according to previous studies [9,22,29]. Inclusion of relative tough and ductile metallic Fe in the CMC coating improves its toughness. Therefore, the wear resistance of the CMC coating is enhanced. (b) Tribological heat produced by friction during testing was difficult to diffuse and concentrated on the real contact area of friction pairs, which raised the temperature of the Al_2O_3 coating quickly and accelerated the wear of the Al_2O_3 coating [30]. Metallic phase Fe in the CMC coating is, however, an excellent conductor of heat, so the temperature increase of the CMC coating was relatively low, which led to the lower wear volume of the CMC coating. (c) It is known that the smaller the grain size, the higher the external stress required to induce grain boundary cracking and grain pulling out is [6,22]. Refining the coating microstructure to nanostructure allows the CMC coating to exhibit a more ductile behaviour [6,9]. Therefore, the CMC coating presents excellent wear resistance, which is consistent with several previous investigation results [6]. (d) The enhanced grain boundary adhesive strength between second phases and matrix due to *in situ* natural formation of all phases is also contributing to the better wear resistance of the CMC coating compared with the Al_2O_3 coating [19]. Further nanostructure formation mechanism, toughening and reinforcing mechanisms and systematic tribological studies of the CMC coating are under investigation.

4. Conclusions

In situ nanostructured CMC coating can be successfully prepared by reactive plasma spraying micro-sized Al–Fe_2O_3 composite powders. The CMC coating exhibits dense and crack-free microstructure with a number of spherical α-Fe and γ-Al_2O_3 nano-sized grains embedded within the equiaxed and columnar $FeAl_2O_4$ nano-grains matrix. Considerably enhanced toughness and wear resistance of the nanostructured CMC coating compared with the microstructured Al_2O_3 coating are achieved due to the nanostructure of the CMC coating and the inclusion of ductile metallic phase Fe in the CMC coating. The major advantage of this processing route is its simplicity and cost effectiveness which may rapidly lead to mass production and commercial application of nanostructured coating materials.

Acknowledgements

The authors gratefully acknowledge the financial supports of the National Natural Science Foundation of China (Grant Nos. 50772028 and 51072045) and the Natural Science Foundation of Heibei province, China (Grant No. E2009000052).

References

[1] H. Chen, Y. Gao, S. Tao, Y. Liu, H. Luo, J. Alloys Compd. 486 (2009) 391.
[2] C. Li, Y. Wang, L. Guo, J. He, Z. Pan, L. Wang, J. Alloys Compd. 506 (2010) 356.
[3] C. Huang, L. Du, W. Zhang, J. Alloys Compd. 479 (2009) 777.
[4] T. Feng, H. Li, Q. Fu, H. Wu, X. Shen, J. Alloys Compd. 501 (2010) L20.
[5] Y. Yang, Y. Wang, W. Tian, Y. Zhao, J. He, H. Bian, Z. Wang, J. Alloys Compd. 481 (2009) 858.
[6] V. Viswanathan, T. Laha, K. Balani, A. Agarwal, S. Seal, Mater. Sci. Eng. R 54 (2006) 121.
[7] C. Zhou, N. Wang, Z. Wang, S. Gong, H. Xu, Scripta Mater. 51 (2004) 945.
[8] G. Vourlias, N. Pistofidis, P. Psyllaki, E. Pavlidou, G. Stergioudis, K. Chrissafis, J. Alloys Compd. 483 (2009) 378.
[9] P. Bansal, N.P. Padture, A. Vasiliev, Acta Mater. 51 (2003) 2959.
[10] M. Stueber, H. Holleck, H. Leiste, K. Seemann, S. Ulrich, C. Ziebert, J. Alloys Compd. 483 (2009) 321.
[11] D. Zois, A. Lekatou, M. Vardavoulias, A. Vazdirvanidis, J. Alloys Compd. 495 (2010) 611.
[12] G. Vourlias, N. Pistofidis, P. Psyllaki, E. Pavlidou, G. Stergioudis, K. Chrissafis, J. Alloys Compd. 483 (2009) 382.
[13] C. Li, Y. Wang, S. Wang, L. Guo, J. Alloys Compd. 503 (2010) 127.
[14] L. Pawlowski, Surf. Coat. Technol. 202 (2008) 4318.
[15] P.V. Ananthapadmanabhan, P.R. Taylor, J. Alloys Compd. 287 (1999) 121.
[16] G.M. Ingo, S. Kaciulis, A. Mezzi, T. Valente, F. Casadei, G. Gusmano, Electrochim. Acta 50 (2005) 4531.
[17] H. Wang, J. Huang, J. Zhu, H. Zhang, X. Zhao, J. Alloys Compd. 472 (2009) L1.
[18] S.C. Deevi, V.K. Sikka, C.J. Swindeman, R.D. Seals, J. Mater. Sci. 32 (1997) 3315.
[19] E. Galvanetto, F. Borgioli, F.P. Galliano, T. Bacci, Surf. Coat. Technol. 200 (2006) 3650.
[20] V. Pasumarthi, Y. Chen, S.R. Bakshi, A. Agarwal, J. Alloys Compd. 484 (2009) 113.
[21] C. Tekmen, Y. Tsunekawa, M. Okumiya, Surf. Coat. Technol. 203 (2009) 1649.

[22] D. Zois, A. Lekatou, M. Vardavoulias, Surf. Coat. Technol. 204 (2009) 15.
[23] Y. Yang, Y. Wang, W. Tian, Z. Wang, C. Li, Y. Zhao, H. Bian, Scripta Mater. 60 (2009) 578.
[24] J.J. Moore, H.J. Feng, Prog. Mater. Sci. 39 (1995) 275.
[25] L. Duraes, B.F.O. Costa, R. Santos, A. Correia, J. Campos, A. Portugal, Mater. Sci. Eng. A 465 (2007) 199.
[26] J. Mei, R.D. Halldearn, P. Xiao, Scripta Mater. 41 (1999) 541.
[27] P.M. Botta, R.C. Mercader, E.F. Aglietti, J.M. Porto Lopez, Scripta Mater. 48 (2003) 1093.
[28] J. Gurt Santanach, C. Estournes, A. Weibel, A. Peigney, G. Chevallier, Ch. Laurent, Scripta Mater. 60 (2009) 195.
[29] L.L. Shaw, D. Goberman, R. Ren, M. Gell, S. Jing, Y. Wang, T.D. Xiao, P.R. Strutt, Surf. Coat. Technol. 130 (2000) 1.
[30] Z. Yin, S. Tao, X. Zhou, C. Ding, Appl. Surf. Sci. 54 (2008) 1636.